Low-Temperature Magnetic Ordering in Rare-Earth Copper Germanates $R_2CuGe_4O_{12}$, R = Ho, Er

C. Cascales,*,† M. T. Fernández Díaz,†,‡ and M. A. Monge†

Instituto de Ciencia de Materiales de Madrid, CSIC. Cantoblanco, E−28049 Madrid, Spain, and Institut Laue Langevin, BP 156 X, F-38042 Grenoble Cedex, France

Received July 3, 2000. Revised Manuscript Received August 25, 2000

$R_2CuGe_4O_{12}$ (R = Y, Ho, Er) have been prepared in polycrystalline form, and crystal structures of both lanthanide-containing compounds have been refined from room-temperature high-resolution neutron diffraction data. These materials are isostructural, with the symmetry of the triclinic space group $P\bar{1}$ (No. 2), $Z = 1$, and unit cell parameters a (Å) = 7.1678 (1) and 7.1594 (2); b (Å) = 7.9291 (1) and 7.9205 (2); c (Å) = 4.89409 (8) and 4.9075 (1); α (°) = 86.874 (1) and 86.926 (2); β = (°) 102.686 (1) and 102.651 (2); γ (°) = 113.792 (1) and 113.735 (2), for R = Ho and Er, respectively. The structure can be depicted as formed by chains of RO_7 polyhedra running in the a direction, layers parallel to the ab plane of tetrameric $(GeO_4)_4$ units, and isolated CuO_6 distorted octahedra which connect these units in the c direction as well as the RO_7 chains along b. Magnetic susceptibility measurements between 350 and 1.7 K reveal for Ho and Er compounds the existence of one anomaly appearing at $T_1 = 3.3$ K in both cases. From low-temperature neutron diffraction data, three-dimensional (3D) antiferromagnetic (AF) ordering in these compounds is established, with a simultaneous setting up of the order for R^{3+} and Cu^{2+} sublattices at $T_N = T_1$. The propagation vectors of the magnetic structures are $\mathbf{k} = [0, 0, {}^1/_2]$ and $[0, {}^1/_2, {}^1/_2]$ for R = Ho and Er, respectively. For the first compound, the best fit of the 1.6 K experimental neutron diffraction data is favorably explained by the ferromagnetic coupling between all Ho^{3+} and Cu^{2+} magnetic moments within ab planes, with a 3D AF coupling along the c direction. For $Er_2CuGe_4O_{12}$, the ferromagnetic arrangement of Er^{3+} and Cu^{2+} magnetic moments is observed only in the a direction, whereas along the two other axes they show AF coupling.

Introduction

The surprising structural diversity of copper oxide compounds, especially with respect to the particular topologies of the corresponding spin networks constituted by Cu^{2+} ions, makes these materials very useful as model systems for fundamental studies of low-dimensional magnetism. From this point of view, the discovery of the spin-Peirls transition in $CuGeO_3$,[1] and the description of weakly interacting isolated antiferromagnetic (AF) dimers in $CaCuGe_2O_6$,[2,3] triggered the search for new singlet ground-state compounds in families of copper germanates and silicates. Examples of other copper arrangements besides the above-mentioned $CuGeO_3$ (linear chains, spin Peierls) and $CaCuGe_2O_6$ (zigzag chains, dimerized ground state) have recently been found in $BaCuSi_2O_6$ (square-lattice bilayer of $S = {}^1/_2$ sites, singlet ground state, and temperature-dependent spin gap[4]), in isostructural $BaCu_2Si_2O_7$ and $BaCu_2Ge_2O_7$ compounds[5] (zigzag chain network of corner-sharing CuO_4 plaquettes, giving raise to weakly coupled $S = {}^1/_2$ chains, showing a crossover from one-dimensional, 1D, behavior at high temperatures to 3D behavior and long-range AF order below the Néel temperature T_N, for the Si compound, or weak ferromagnetic spin arrangement below T_N, for the germanate), and in $K_2Cu_3Ge_5O_{14}$ (chains of edge-sharing CuO_6 octahedra and CuO_5 square pyramids along the [1 0−1] direction, showing a deviation from the Curie−Weiss law below 30 K).[6]

On the other hand, "pure" rare earth R-germanates[7−15] along with mixed metal M- and R-germanates possess-

* Fax: 34 91 3720623. E-mail: ccascales@icmm.csic.es.
† Instituto de Ciencia de Materiales de Madrid.
‡ Institut Laue Langevin.

(1) Hase, M.; Terasaki, I.; Uchinokura, K. *Phys. Rev. Lett.* **1993**, *70*, 3651.
(2) Sasago, Y.; Hase, M.; Uchinokura, K.; Tokunaga, M.; Miura, N. *Phys. Rev. B* **1995**, *52*, 3533.
(3) Zheludev, A.; Shirane, G.; Sasago, Y.; Hase, M.; Uchinokura, K. *Phys. Rev. B* **1996**, *53*, 11642.
(4) Sasago, Y.; Uchinokura, K.; Zheludev, A.; Shirane, G. *Phys. Rev. B* **1997**, *55*, 8357.
(5) Tsukada, I.; Sasago, Y.; Uchinokura, K.; Zheludev, A.; Maslov, S.; Shirane, G.; Kakurai K.; Ressouche, E. *Phys. Rev. B* **1999**, *60*, 6601.
(6) Monge, M. A.; Gutiérrez Puebla, E.; Cascales, C.; Campá, J. A. *Chem. Mater.* **2000**, *12*, 1926.
(7) Demianets, L. N.; Lobachev, A. N.; Emelchenko, G. A. *Germanates of Rare-Earths Elements*; Nauka: Moscow, 1980.
(8) Chigarov, M. I.; Mamedov, K. S.; Kulieva, T. Z. *Kristallografiya* **1983**, *28*, 1035.
(9) Vetter, G.; Queyroux, F.; Labbe, P.; Goreaud, M. *J. Solid State Chem.* **1982**, *45*, 293.
(10) Brixner, L.; Calabrese, J.; Chen, H. Y. *J. Less-Common Met.* **1985**, *110*, 397.
(11) Geller, S.; Gaines, J. M. *Z. Kristallogr.* **1987**, *180*, 243.
(12) Demianets, L. N.; Radaev, S. F.; Mamin, B. F.; Maksimov, B. A. *Zh. Strukt. Khim.* **1988**, *29*, 150.
(13) Palkina, K. K.; Kuzmina, N. E.; Lysanova, G. V.; Dzhurinskii, B. F.; Komova, M. G. *Zh. Neorg. Khim.* **1994**, *39*, 184.
(14) Palkina, K. K.; Kuzmina, N. E.; Dzhurinskii, B. F. *Zh. Neorg. Khim.* **1995**, *40*, 1449.
(15) Jarchow, O.; Klaska, K.-H.; Ruks, M.; Holtz, B. *Z. Kristallogr.* **1996**, *211*, 4.

10.1021/cm0011209 CCC: $19.00 © 2000 American Chemical Society
Published on Web 11/02/2000

ing valuable physical, especially magnetic and optical, properties have found broad applications for a long time. However, most of these studies concern mixed alkali[7,16−18] and alkaline-earth R-germanates,[7,19] and it has been only very recently that reports involving di- or trivalent transition metals from 3rd or 4th periods have appeared.[23−33] Among them, those on germanates with stoichiometry $RMGe_2O_7$, in which M and R represent trivalent metals and rare earths, respectively, indicate different structures depending on the composition. Thus, the monoclinic $NdAlGe_2O_7$ structure-type, space group (SG) $P2_1/c$ (No. 14), has been described[20−22] for compounds with M = Al or Ga and R = a large rare earth. Detailed studies on optical absorption and photoluminescence were carried out for these Pr^{3+} and Nd^{3+} materials,[22−24] as well as on stimulated emission for some Nd compounds.[22] Along the corresponding iron family, the phase formation results are dependent on the size of R, with two different monoclinic crystal structures: the above-mentioned monoclinic type for the larger R cations, R = La to Gd,[22,25−26] and a novel structure type,[27] $YFeGe_2O_7$, SG $P2_1/m$ (No. 11), recently determined for the smaller ones.[28] Magnetic properties, including the determination of their magnetic structures, have been reported for both kinds of iron germanates.[26−29] Also in this group, $GdMnGe_2O_7$ has been very recently been found to crystallize in the orthorhombic SG $A222$ (No. 21).[30] Unfortunately, the physical properties of materials reported in references[30−33] have not yet been described.

The awareness of the lack of available information on single crystals of germanates containing copper and rare earths led some of the authors to the study of the Cu−R−Ge−O system. The growth for the first time of crystals of two series of these germanates, $R_2CuGe_2O_8$ and $R_2CuGe_4O_{12}$, with R = Nd and Yb, respectively, allowed them to establish their corresponding crystallographic structures, with monoclinic SG Cm (No. 8),[34] and triclinic SG $P\bar{1}$ (No. 2)[35] symmetries. Moreover, since very interesting physical properties and possible applications can be expected for these compounds insofar as they contain new arrangements of magnetic copper and lanthanide cations not yet seen, measurements of the magnetic properties of these materials were performed. In particular, in the last family, magnetic susceptibility χ measurements from 350 to 1.8 K on $Yb_2CuGe_4O_{12}$ clearly displayed deviations from linearity over the whole measured range; nevertheless, no maxima in χ were observed at low temperatures, even when a weak magnetic field of 10 Oe was applied.[35] This indicate that although the antiferromagnetic ordering of both R^{3+} and Cu^{2+} sublattices is not completely reached for this Yb compound or, at least, it cannot be observed from magnetic susceptibility measurements, the reduction in the paramagnetic moment when the temperature decreases should be justified by magnetic interactions inducing some short-range magnetic order which gradually appears in it.

The aim of this article is therefore to characterize the microscopic magnetic behavior of isostructural compounds $R_2CuGe_4O_{12}$, R = Ho and Er. The synthesis of these germanates, the refinement of their crystal structures, and low-temperature neutron diffraction studies were undertaken to investigate the nature of the anomalies displayed by the magnetic measurements and to determine the magnetic structure of the low-temperature phases.

Experimental Section

Preparation of the Samples. $R_2CuGe_4O_{12}$ (R = Y, Ho, Er) were prepared as polycrystalline powders by solid-state reaction from analytical-grade mixture of the stoichiometrically required amounts of CuO, GeO_2, and R_2O_3, with a slight excess of the Ge oxide in order to counteract their losses especially as a vitrified product. Samples were ground and heated in air to final temperatures of 1273 K over 2 weeks. Standard X-ray powder diffraction analysis indicated that final samples were well-crystallized and appeared, to the limit of the technique, free of other crystalline phases.

Crystal and Magnetic Structure Refinements. Neutron powder diffraction (NPD) patterns were collected on the D1B, D1A, and D2B powder diffractometers, at the ILL-Grenoble, using wavelengths of 2.524, 1.911, and 1.595 Å, respectively. About 8 g of sample contained in a cylindrical vanadium can was used in each case. The high flux and medium resolution of D1B were employed to study the thermal evolution of these three materials, in the temperature range 1.6−10 K, with the vanadium can held in a liquid helium cryostat. The diffraction patterns were collected every 1 K over the angular range $5° \leq 2\theta \leq 85°$, in steps of 0.2° 2θ. To obtain more accurate data, the lowest temperature pattern consists of the integration of several measured patterns at 1.6 K. High-resolution D2B (for R = Ho) and D1A (R = Er) diffractometers were used to obtain more extensive and accurate data of these two compounds at room temperature, over a large angular range $5° \leq 2\theta \leq 155°$, in steps of 0.05° 2θ.

The Rietveld method was used to refine the crystal and magnetic structures. All of the data were analyzed with the program WinPLOTR.[36] A pseudo-Voigt function was chosen

(16) Merinov, B. V.; Maksimov, B. A.; Demianets, L. N.; Belov, N. V. *Dokl. Akad. Nauk SSSR* **1980**, *250*, 357.
(17) Malinovskii, Yu. A.; Bondareva, O. S. *Zh. Strukt. Khim.* **1991**, *32* (4), 173.
(18) Dudka, A. P.; Kaminskii, A. A.; Simonov, V. I. *Phys. Status Solidi A* **1986**, *93*, 495.
(19) Malinovskii, Yu. A.; Belokoneva, E. L.; Demianets, L. N. *Zh. Strukt. Khim.* **1991**, *32* (3), 173.
(20) Jarchow, O.; Klaska, K.-H.; Schenk-Strauss, H. *Z. Kristallogr.* **1985**, *172*, 159.
(21) Mill, B. V.; Kazei, S. A.; Reiman, S. Y.; Tamazyan, S. A.; Khamdamov, F. D.; Bykova, L. Yu. *Vestn. Mosk. Gos. Univ. Fiz. Astron.* **1987**, *28*, 95.
(22) Kaminskii, A. A.; Mill, B. V.; Butashin, A. V.; Belokoneva, E. L.; Kurbanov, K. *Phys. Status Solidi* **1987**, *103*, 575.
(23) Lozano, G.; Cascales, C.; Zaldo, C.; Porcher, P. *J. Alloys Compd.* **2000**, *303−304*, 349.
(24) Cascales, C.; Lozano, G.; Zaldo, C.; Porcher, P. *Chem. Phys.* **2000**, *257*, 49.
(25) Bucio, L.; Cascales, C.; Alonso, J. A.; Rasines, I. *J. Phys.: Condens. Matter* **1996**, *8*, 2641.
(26) Cascales, C.; Bucio, L.; Gutiérrez Puebla, E.; Rasines, I.; Fernández Díaz, M. T. *J. Alloys Compd.* **1998**, *275*, 629.
(27) Kazei, Z. A.; Kuyanov, Z. A., Levitin, R. Z.; Markosyan, A. S.; Mill, B. V.; Reiman, S. Y.; Snegirev V. V.; Tamazyan, S. A. *Sov. Phys. Solid State* **1989**, *31*, 233.
(28) Cascales, C.; Bucio, L.; Gutiérrez Puebla, E.; Rasines, I.; Fernández Díaz, M. T. *Phys. Rev. B* **1998**, *57*, 5240.
(29) Cascales, C.; Gutiérrez Puebla, E.; Klimin, S.; Lebech, B.; Monge, A.; Popova, M. N. *Chem. Mater.* **1999**, *11*, 2520.
(30) Taviot-Guého, C.; Leone, P.; Palvadeau, P.; Rouxel, J. *J. Sol. State Chem.* **1999**, *143*, 145.
(31) Adiwidjaja, G.; Broeker, M.; Claus, C.; Friese, K.; Klaska, K.-K.; Jarchow, O.; Ruks, M.; Wozniak, I. *Z. Kristallogr.* **1998**, *213*, 223.
(32) Gueho, C.; Giaquinta, D.; Palvadeau, P.; Rouxel, J. *J. Sol. State Chem.* **1995**, *120*, 7.
(33) Chandley, P.; Clark, R. J. H.; Angel, R. J.; Price, G. D. *J. Chem. Soc., Dalton Trans.* **1992**, 1579.
(34) Campá, J. A.; Gutiérrez Puebla, E.; Monge, A.; Ruíz Valero, C.; Mira, J.; Rivas, J.; Cascales, C.; Rasines, I. *J. Sol. State Chem.* **1995**, *120*, 254.
(35) Campá, J. A.; Cascales, C.; Gutiérrez Puebla, E.; Monge, A.; Rasines, I.; Ruiz Valero, C. *J. Solid State Chem.* **1996**, *124*, 17.

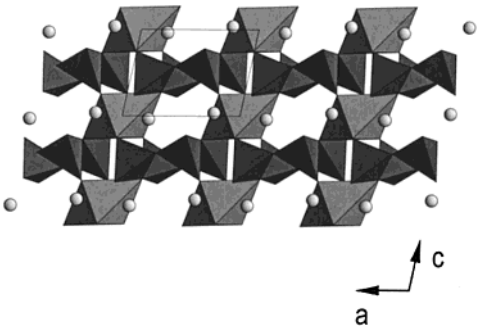

Figure 1. View of the lattice of $R_2CuGe_4O_{12}$ along the *b* direction, showing connections between $[(GeO_4)_4]_n$ (deep gray) tetrahedra layers through isolated CuO_6 octahedra (medium gray) in the *c* direction. Spheres represent R^{3+} cations.

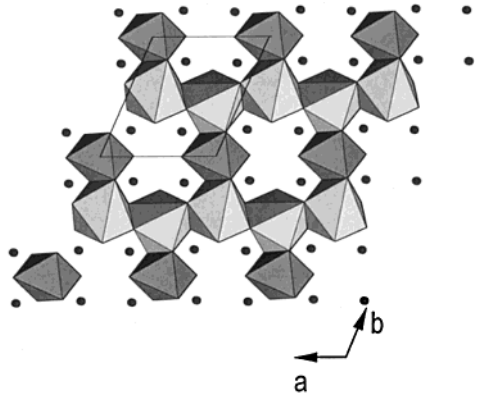

Figure 2. Chains running along the *a* axis of RO_7 (light gray) polyhedra, linked in the *b* direction through CuO_6 octahedra. Small spheres represent Ge positions.

to generate the line shape of the diffraction peaks. The background was fitted to a polynomial refinable function. Crystal structures at room temperatures were refined taking as starting parameters those previously obtained from X-ray single-crystal data for $Yb_2CuGe_4O_{12}$.[35] D1B diffraction patterns taken at increasing temperatures were refined sequentially, with starting parameters for each pattern those resulting from the refinement of the preceding one at lower temperature.

Magnetic Measurements. A SQUID magnetometer (Quantum Design) operating from 350 to 1.7 K at 100 Oe was used to carry out direct current magnetic susceptibility measurements. Diamagnetic corrections[37] for the magnetic susceptibilities were taken into account.

Crystal Structure of $R_2CuGe_4O_{12}$, R = Ho, Er

The $R_2CuGe_4O_{12}$ structure type, where R is a smaller rare-earth, typically Y and Eu to Lu,[38] has been described by single-crystal X-ray diffraction for the Yb compound in a previous work.[35] It presents the triclinic symmetry of the space group $P\bar{1}$ (No. 2), $Z = 1$. In this structure, Ge atoms exhibit the usual tetrahedral coordination, Cu atoms are situated in inversion centers with an elongated octahedral coordination, for which apical oxygen atoms are at distances very similar to those found in $CuGeO_3$, and R atoms are seven-coordinated, forming RO_7 C_{3v}-capped octahedra. Every four GeO_4 tetrahedra are associated by sharing vertexes, forming tetrameric $(GeO_4)_4$ units, in an alternate configuration. The structure contains layers parallel to the *ab* plane of these $(GeO_4)_4$ units, and although there is no direct joining between them, they are connected in the *c* direction through isolated CuO_6 octahedra, as shown in Figure 1. Since the apical Cu−O3 distance in the above octahedra is somewhat larger than the two others, planar-square oxygen coordination could be also considered for Cu atoms. Chains of sharing-edge RO_7 polyhedra are running parallel to the *a* direction, and they are linked along the *b* direction through $(GeO_4)_4$ units and CuO_6 octahedra, as depicted in Figure 2. Further details on this structure type are described elsewhere.[35]

Table 1. Lattice Parameters and Discrepancy Factors for $R_2CuGe_4O_{12}$, R = Ho, Er, $P\bar{1}$ (No. 2), $Z = 1$

	Ho		Er	
lattice param.				
a (Å)	7.1678(1)[a]	7.1688(9)[b]	7.1594(2)[c]	7.141(2)[b]
b (Å)	7.9291(1)	7.913(1)	7.9205(2)	15.756(2)
c (Å)	4.89409(8)	9.7914(8)	4.9075(1)	9.793(2)
α (°)	86.874(1)	87.07(1)	86.926(2)	87.15(1)
β (°)	102.686(1)	102.45(1)	102.651(2)	102.44(1)
γ (°)	113.792(1)	113.63(1)	113.735(2)	113.57(3)
no. reflections	993	159	561	156
reliabil. factors (%)				
χ^2	2.46	23.6	2.72	47.8
R_p	2.36	2.35	4.36	3.80
R_{exp}	1.91	0.64	3.34	0.77
R_{Bragg}	3.29	4.73	5.37	8.23
R_f	1.85	3.62	3.19	5.74
R_{mag}		3.56		9.57

[a] From RT D2B NPD data. [b] 1.6 K D1B NPD data. [c] RT D1A NPD data.

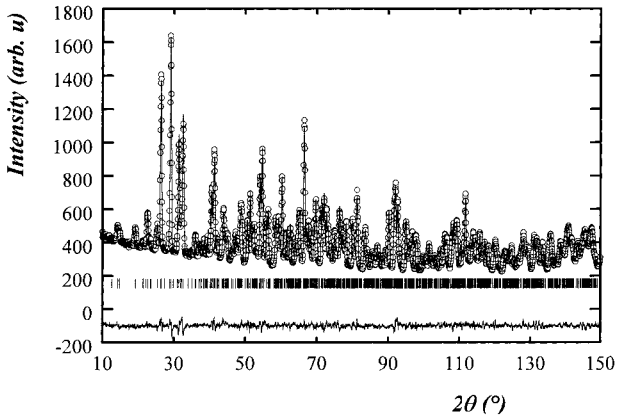

Figure 3. Observed, calculated, and difference neutron diffraction (D2B, ILL) profiles of $Ho_2CuGe_4O_{12}$ at room temperature. Vertical marks correspond to the position of the allowed Bragg reflections for the crystallographic structure.

Table 1 includes the crystal parameters for both Ho and Er compounds, obtained from NPD data at room temperature. Figure 3 shows the observed and calculated profiles at this temperature for $Ho_2CuGe_4O_{12}$. The final refined positional and thermal parameters for both germanates are given in Table 2, and Table 3 consists of the main interatomic distances, including the intermetallic ones, R−R along *a* and *c* directions, and distances between Cu and RO_7 chains.

Magnetic Susceptibility Measurements

Figures 4 and 5 show the variation with temperature of the molar magnetic susceptibility χ_m for $R_2CuGe_4O_{12}$,

(36) Roisnel, T.; Rodríguez Carvajal, J. *WinPLOTR Program for Rietveld Refinement and Pattern Matching Analysis*; Laboratoire Léon Brillouin, CEA-CNRS, Centre d'Etudes de Saclay: France, 1999.
(37) Boudreaux, E. A.; Mulay, L. N. *Theory and Applications of Molecular Paramagnetism*; Wiley: New York, 1976; pp 494−5.
(38) Lambert, U.; Eysel, W. *Powder Diffract.* **1986**, *1*, 256.

Table 2. Final Refined Positional and Thermal Parameters for $R_2CuGe_4O_{12}$, R = Ho, Er

	x/a	*y/b*	*z/c*	*B* (Å^2)[a]
Ho	0.2307(3)	0.4512(3)	0.0435(4)	0.14(4)
Ge(1)	0.3808(3)	0.2057(3)	−0.4210(4)	0.61(3)
Ge(2)	0.1674(3)	0.7778(3)	−0.4572(4)	0.68(3)
Cu	0	0	0	0.87(8)
O1	0.2239(4)	0.1908(4)	−0.7456(6)	0.72(4)
O2	−0.0034(4)	0.7981(4)	−0.7529(6)	0.57(4)
O3	0.3004(5)	−0.0086(4)	−0.2676(6)	1.22(4)
O4	0.3474(5)	0.7166(5)	0.4222(7)	1.33(4)
O5	0.4242(5)	0.3918(4)	−0.2146(6)	0.95(4)
O6	0.0647(5)	0.6109(4)	−0.2268(6)	0.88(4)
Er	0.2305(6)	0.4500(5)	0.0435(8)	0.03(8)
Ge(1)	0.3839(5)	0.2073(5)	−0.4196(8)	0.19(5)
Ge(2)	0.1675(5)	0.7785(5)	−0.4586(8)	0.19(5)
Cu	0	0	0	0.39(12)
O1	0.2242(7)	0.1929(7)	−0.7397(10)	0.16(5)
O2	−0.0005(8)	0.8003(7)	−0.7538(10)	0.16(5)
O3	0.3029(7)	−0.0072(6)	−0.2688(10)	0.16(5)
O4	0.3471(7)	0.7202(7)	0.4227(11)	0.16(5)
O5	0.4271(7)	0.3940(7)	−0.2130(11)	0.16(5)
O6	0.0634(8)	0.6084(8)	−0.2291(10)	0.16(5)

[a] Isotropic thermal parameters for O atoms in $Er_2CuGe_4O_{12}$ have been constrained on the same value.

Table 3. Main Interatomic Distances (Å) in $CuR_2Ge_4O_{12}$, R = Ho, Er

	Ho	Er		Ho	Er
Ge1−O1	1.712(3)	1.708(6)	R−O1	2.245(3)	2.235(6)
Ge1−O3	1.744(4)	1.741(6)	R−O2	2.297(3)	2.305(6)
Ge1−O4	1.792(4)	1.778(7)	R−O4	2.624(4)	2.655(6)
Ge1−O5	1.717(4)	1.723(6)	R−O5	2.259(4)	2.258(7)
Ge2−O2	1.725(4)	1.718(6)	R−O5	2.256(4)	2.237(7)
Ge2−O3	1.766(4)	1.771(6)	R−O6	2.260(4)	2.264(7)
Ge2−O4	1.766(5)	1.744(7)	R−O6	2.339(4)	2.341(7)
Ge2−O6	1.727(4)	1.742(6)	R−R, *c*	4.894(3)	4.907(6)
Cu−O1 × 2	1.945(3)	1.969(5)	R−R, *a*	3.623(3)	3.627(6)
Cu−O2 × 2	1.949(3)	1.937(5)	R−R, *a*	3.737(3)	3.731(6)
Cu−O3 × 2	2.779(4)	2.794(5)	Cu−R	3.276(2)	3.266(4)

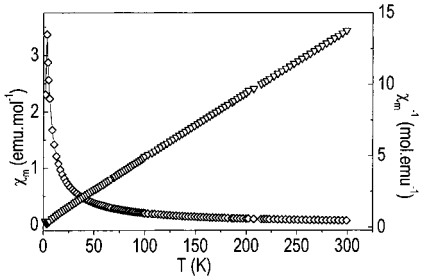

Figure 4. Thermal evolution of the molar magnetic susceptibility χ_m and its reciprocal χ_m^{-1} for $Ho_2CuGe_4O_{12}$.

R = Ho, Er. For each compound, a clear maximum is observed at very low temperatures, 3.3 K, in both cases. These peaks could be related to transitions to antiferromagnetically ordered states of the Cu^{2+} and R^{3+} magnetic sublattices.

At temperatures from ∼20 K up to room temperature, Curie−Weiss behavior is observed in both cases, χ_m^{-1} = 0.151(3) + 0.037 02(2) T mol emu^{-1} (r = 0.999 99), and 0.380(8) + 0.04491(5) T mol emu^{-1} (r = 0.999 95), with paramagnetic Curie temperatures θ_c = −4.07(7) and −8.5(2) K and effective magnetic moments μ_{eff} = 14.66(5) and 13.4(1) μ_B, for Ho and Er compounds, respectively.

To consider the magnetic behavior of an isostructural compound with only the magnetic subsystem of Cu^{2+} cations, the variation with the temperature of the

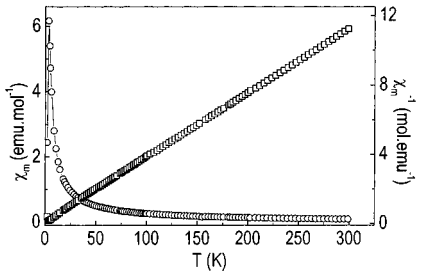

Figure 5. Molar magnetic susceptibility $\chi_m(T)$ and its reciprocal $\chi_m^{-1}(T)$ for $Er_2CuGe_4O_{12}$.

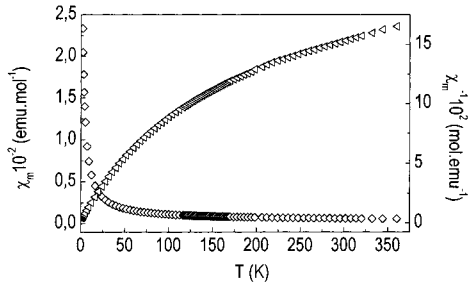

Figure 6. Molar magnetic susceptibility $\chi_m(T)$ and its reciprocal $\chi_m^{-1}(T)$ for $Y_2CuGe_4O_{12}$.

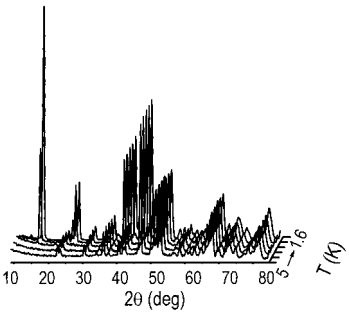

Figure 7. Evolution of the neutron powder diffraction patterns of $Ho_2CuGe_4O_{12}$ between 1. 6 and 5 K.

paramagnetic susceptibility for $Y_2CuGe_4O_{12}$ was also measured. As it can be observed in Figure 6, the plot presents a deviation from linearity over the whole measured range, stronger below 100 K, but any maximum is observed at low temperature. The calculated magnetic moment at room temperature is 1.77(3) μ_B, and the paramagnetic temperature results are very large and negative, −297 K.

Magnetic Ordering in $R_2CuGe_4O_{12}$, R = Ho, Er

The evolution of the NPD patterns for both $R_2CuGe_4O_{12}$, R = Ho, Er, in a range for the 2θ scattering angle from 8° to 85° and temperatures from 1.6 to 5 K is presented in Figures 7 and 8. Analogously, Figure 9 shows NPD patterns for $Y_2CuGe_4O_{12}$ at 1.6 and 12 K, i.e., above and below the Néel temperature for the other two lanthanide compounds. Comparison of both temperature collected data did not reveal any sign of magnetic Bragg reflections. This failure to observe any magnetic signal is not surprising for a structure where *isolated* CuO_6 are arranged between *a*-running RO_7 chains, the nearest-neighbor in-plane Cu−Cu distances being large, ∼7.1 and ∼7.9 Å, equal to the *a* and *b* lattice constants, respectively; see Figure 2.

Conversely, for both compounds containing magnetic R cations, a different series of extra peaks begins to

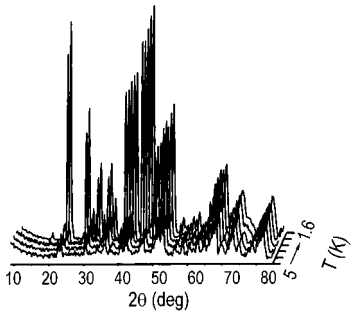

Figure 8. Thermal evolution between 1. 6 and 5 K of the neutron powder diffraction patterns of $CuEr_2Ge_4O_{12}$.

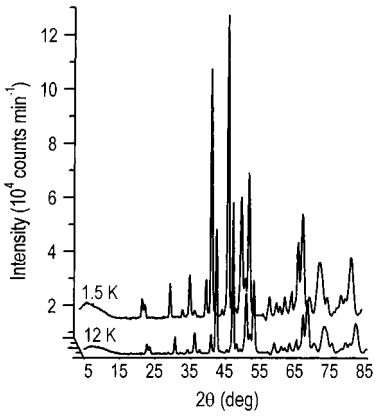

Figure 9. Neutron powder diffraction patterns of $Y_2CuGe_4O_{12}$ at 1. 6 and 12 K.

appear below 3 K, a temperature that corresponds to the observed maxima in χ versus T curves. The intensities of the magnetic reflections grow regularly up to the lowest temperature, 1.6 K. The developing intensity of the AF magnetic peaks is associated with a reduction of the background due to the ordering of the paramagnetic ions. The appearance of such strong magnetic peaks at a quite low temperature indicates the magnetic ordering of the rare-earth sublattice of both compounds.

The careful analysis of Bragg peaks in the NPD patterns reveals that for $Ho_2CuGe_4O_{12}$ below 3 K the observed peaks in the 2θ range 8°−85° can be indexed within a commensurate lattice with unit cell parameters $a' = a$, $b' = b$, and $c' = 2c$, a, b, and c being the parameters of the crystallographic unit cell; that is, the 3D long-range ordered magnetic structure can be described in terms of a single propagation vector $\mathbf{k} = [0, 0, {}^1/_2]$. However, besides this series of extra peaks, and only in the lowest temperature pattern, a unique reflection is detected at ∼11.7°, with very weak intensity. Its origin will be discussed below.

For $Er_2CuGe_4O_{12}$ and upon cooling below 3 K, the observed Bragg peaks in the NPD patterns were indexed within a commensurate lattice whose unit cell parameters are $a' = a$, $b' = 2b$, and $c' = 2c$; thus in this case, the 3D AF-ordered magnetic structure can be described in terms of a single propagation vector $\mathbf{k} = [0, {}^1/_2, {}^1/_2]$. Contrary to the case of the Ho compound, no signal of the appearance of additional reflections was observed.

Group-Theory Analysis for $R_2CuGe_4O_{12}$, R = Ho, Er

The nuclear unit cell of $R_2CuGe_4O_{12}$ contains two R atoms located at 2*i* general positions and one Cu atom at (0, 0, 0). Since the lattice is primitive, the magnetic structure can be described by considering the magnetic moments of one R and one Cu atom, and the remaining magnetic moments can be deduced by means of the $\mathbf{t}_N$ Bravais translation vector, according to $m_{jN} = m_{jO}e^{-2\pi i\mathbf{k}\mathbf{t}_N}$.

Table 4. Character of the Irreducible Representations of $G_k(\bar{1})$

rep.	*E*	*i*
A_g	1	1
A_u	1	−1

The possible magnetic structures compatible with the crystal symmetry can be obtained from the group-theory analysis.[39] All possible forms of ordering of the magnetic moments are determined through the base functions of the irreducible representations of the wave vector group $\mathbf{G_k}$, which contains only those symmetry operations of the high-temperature space group ($T > T_N$) that keep invariant the propagation vector or transforms it into an equivalent vector. In the current case they are the identity and the inversion, $\{E, i\}$. Because of the axial character of the pseudovectors of the magnetic moments, a time reversal θ must be considered when the last symmetry operator was applied. The transformation properties of the components of the magnetic moments under the symmetry operations of the group $\mathbf{G_k}(\bar{1})$ define a representation Γ constituted by two 3 × 3 matrices, the last multiplied by the time reversal operator θ, which reverses all components of the magnetic moments, whose traces are 3 and 3 for both symmetry elements. Table 4 gives the characters of the irreducible representations of Γ^ν of $\mathbf{G_k}(\bar{1})$.

The irreducible representations contained in Γ (R^{3+}) and Γ (Cu^{2+}) are, in both cases, $3A_g$. Therefore, there is only one magnetic structure associated to the representation A_g, which is defined by six free parameters, three for each magnetic sublattice.

Results of Magnetic Structure Refinements and Discussion

For the analysis of the low-temperature NPD data of both R = Ho and Er compounds, a two-phase refinement for every temperature was performed. In each case, the crystal structure was refined taking as starting parameters those obtained for the data collected at room temperature with high-resolution data. The magnetic structure was refined as an independent phase for which only magnetic atoms were defined.

As mentioned before, the Y compound does not show long-range magnetic order of Cu^{2+} cations. For this reason, along with the fact that a single transition temperature has been observed in neutron diffraction as well as in magnetic susceptibility data, the analysis of the low-temperature pattern has been started considering the order of the magnetic moments exclusively on the rare-earth sites. However, experimental data at the lowest temperature result are satisfactorily fitted only if the magnetic moments in Cu^{2+} sites also become ordered.

The final refinement for $Ho_2CuGe_4O_{12}$ provides a magnetic structure which consists of the ferromagnetic coupling between all Ho^{3+} along the HoO_7 chains *and*

(39) Bertaut, E. F. *Acta Crystallogr.* A **1968**, *24*, 217.

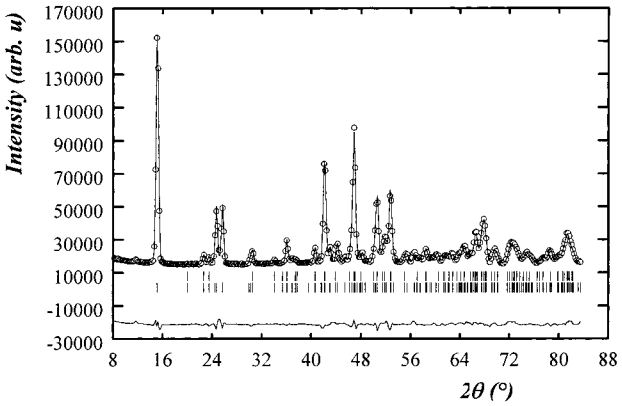

Figure 10. Neutron diffraction pattern of $Ho_2CuGe_4O_{12}$ (D1B, ILL) at 1.6 K. The solid line is the calculated profile and vertical marks correspond to the position of the Bragg reflections for the crystallographic (first row) and magnetic (second row) structures. The difference curve is plotted at the bottom of the figure.

Table 5. Magnetic Moments for R^{3+} and Cu^{2+} in $R_2CuGe_4O_{12}$, R = Ho, Er, at 1.7 K, in Cartesian and Spherical Coordinates

	S_x (μ_B)	S_y (μ_B)	S_z (μ_B)	M (μ_B)	φ (°)	ϕ (°)
Ho^{3+}	5.2(1)	1.0 (2)	1.4(2)	6.10(4)	350.6	244.5
Cu^{2+}	1.1(2)	0.1(2)	0.1(3)	1.05(7)	0.3	287.9
Er^{3+}	2.8(1)	6.3(1)	3.3(2)	6.76(8)	266.6	58.3
Cu^{2+}	0.3(2)	0.5(2)	1.0(2)	1.2(1)	108.5	22.1

Cu^{2+} cations within *ab* planes, being the directions of their magnetic moments nearly aligned, forming small angles up (Cu^{2+}) and down (Ho^{3+}), with the *a* direction. Obviously, along the *c* direction magnetic moments from both magnetic networks are oppositely aligned, as imposed by the propagation vector.

The weak reflection detected at about 11.7° 2θ in the 1.6 K pattern is reproduced through a propagation vector $\mathbf{k} = [1/2, 1/2, 0]$ for the Cu^{2+} sublattice. Despite that, we think that an *independent* long-range magnetic order for the arrangement of Cu^{2+} cations can be discarded as long as the measurements performed on the Y compound hold. More probably, this extra reflection might be originated by the magnetic ordering of traces of Ho_2O_3 present in the prepared sample.

In Figure 10 the observed and final refined patterns at 1.6 K for $CuHo_2Ge_4O_{12}$ are represented. Tables 1 and 5 show a summary of the refined structural parameters and magnetic moments at 1.6 K, respectively. The magnetic moments are written in the Cartesian components allowed by the magnetic structure (S_x, S_y, S_z) as well as in spherical coordinates, with φ and ϕ being the angles of M with *x* and *z* axes, respectively.

The ordered magnetic structure of $Er_2CuGe_4O_{12}$ associated to the A_g irreducible representation is also AF, and as indicated above, it can be described by a single propagation vector $\mathbf{k} = [0, 1/2, 1/2]$, that is, with *b* and *c* axes twice those of the nuclear cell. Between the only two possible arrangements of magnetic moments derived from the different couplings of Er^{3+} and Cu^{2+} sublattices along the *a* direction, the analysis and refinement of the low-temperature NPD data indicates that the magnetic structure of $Er_2CuGe_4O_{12}$ consists of the ferromagnetic arrangement of all of these moments along *a*, with those of Er^{3+} from ErO_7 chains nearly perpendicular to this direction. In this way, the 3D AF ordering arises from the opposite disposition of magnetic moments along the two other axes.

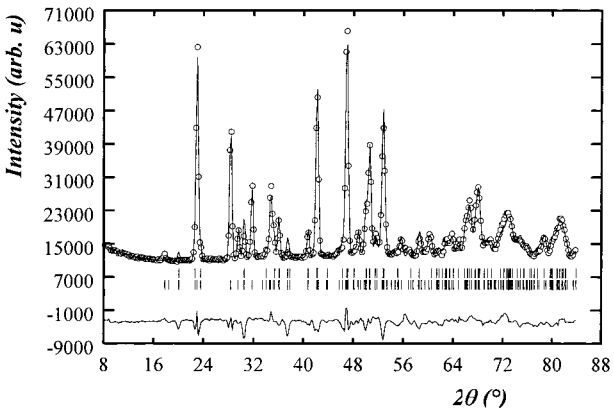

Figure 11. Neutron diffraction pattern of $Er_2CuGe_4O_{12}$ (D1B, ILL) at 1.6 K. The solid line is the calculated profile and vertical marks correspond to the position of the Bragg reflections for the crystallographic (first row) and magnetic (second row) structures. The difference curve is plotted at the bottom of the figure.

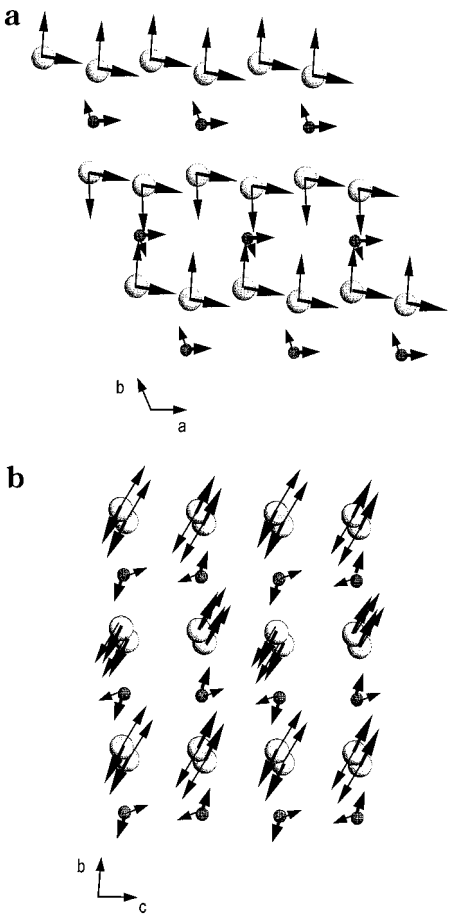

Figure 12. Projection of the arrangement of magnetic moments of R and Cu onto (a) *ab* and (b) *bc* planes. Small and large spheres are representing Cu and R atoms, and thick and thin arrows correspond to Ho and Er, respectively.

In Figure 11, observed and calculated patterns at 1.6 K for $Er_2CuGe_4O_{12}$ are represented. A summary of final refined structural parameters and magnetic moments at this temperature is also shown in Tables 1 and 5, respectively.

For both compounds, values of the ordered moments M of the rare-earth are lower than those expected for

free ions, 10.6 and 9.6 μ_B, for Ho^{3+} and Er^{3+}, respectively. Actually, magnetic peaks in 1.6 K NPD spectra have not yet reached their maximum intensities, and therefore, the strong reduction in M is not surprising; i.e., these values correspond to nonsaturated magnetic moments.

Figure 12a shows a schematic view of the disposition of the magnetic moments for both Ho and Er compounds on the *ab* plane, and Figure 12b shows the corresponding projections onto the *bc* plane.

From current results, we can conclude that for $Y_2CuGe_4O_{12}$ only short-range magnetic fluctuations of the Cu^{2+} magnetic system (isolated CuO_6 octahedra) are observed. They seem to develop at around 200 K as can be deduced from the observed deviation of a Curie−Weiss law in the χ versus T curve. However, their long-range order is not reached even at low temperatures. In $R_2CuGe_4O_{12}$ isostructural compounds, when R is a magnetic rare-earth such as Ho or Er, the order of rare-earth magnetic moments is due to R−R interactions, which take place at very low temperatures. The magnetic order in the R-system would induce the ordering of the copper moments, through R−Cu interactions, with a simultaneous setting up of the order for both R^{3+} and Cu^{2+} sublattices, and the same propagation vector. In short, in this structure, it is the connection between chains of magnetic rare-earth RO_7 polyhedra through CuO_6 octahedra which creates the adequate pathway for magnetic interactions between both kind of magnetic cations, leading thus to the low-temperature 3D AF ordering of the structure. The magnetic behavior of studied $R_2CuGe_4O_{12}$ germanates is dominated by the paramagnetic rare earth and depending on R the compound is going to adopt a different magnetic structure, which is defined in each case by its **k** propagation vector, and moreover different directions of the anisotropy of R will be reflected in highly anisotropic Cu−R interactions.

Acknowledgment. The authors acknowledge the financial support of the Spanish DGESIC and CICYT under Projects PB97-1200 and MAT99-0892, respectively, and the Institut Laue Langevin for neutron facilities offered.

CM0011209